Graphical Abstract

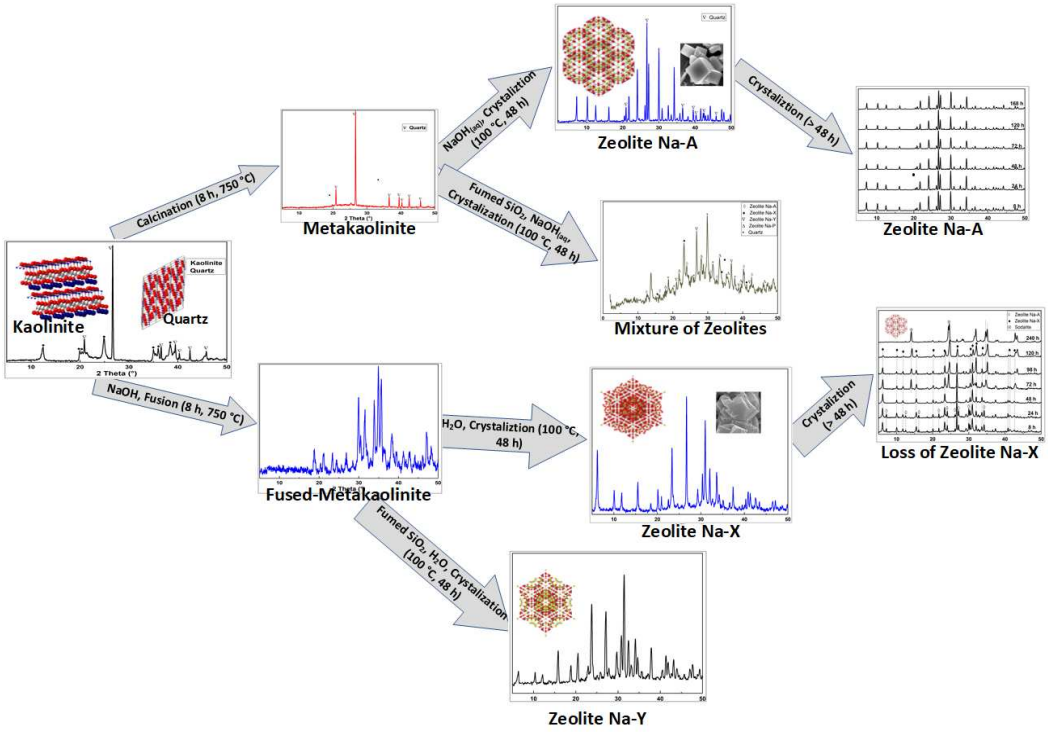

The effects of metakaolinization and fused-metakaolinization on zeolites synthesized from quartz rich natural clays

Stephen O. Otieno[1], Fredric O. Kengara[1], Justin C. Kemmegne-Mbouguen[2], Henrietta W. Langmi[3,4], Chrispin B. O. Kowenje[1*], Robert Mokaya[5*]

[1]Department of Chemistry, Maseno University, P. O. Box, 333- 40105, Maseno - Kenya.
[2]Department of Inorganic Chemistry, University of Yaoundé 1, Cameroon.
[3]HySA Infrastructure Centre of Competence, Energy Centre, Council for Scientific & Industrial Research (CSIR), P. O. Box 395 Pretoria 0001 South Africa
[4]Department of Chemistry, University of Pretoria, Private Bag X20 Hatfield 0028, South Africa
[5]School of Chemistry, University of Nottingham, University Park, Nottingham, NG7 2RD

*****Corresponding author. **ckowenje@maseno.ac.ke, r.mokaya@nottingham.ac.uk**

Abstract

A variety of zeolites have been synthesized by performing either metakaolinization or fused-metakaolinization of natural clays prior to the hydrothermal synthesis step. To understand the differences arising from performing fused metakaolinization rather than simple metakaolinization, the calcination conditions, gel composition, gelling and crystallization conditions were kept similar for both methods. The original clay material, a kaolinite group mineral with Si/Al molar ratio of 1, had a high content of quartz as impurity. The two treatment methods gave different zeolites of high crystallinity and relatively similar Si/Al molar ratio. Zeolite Na-A with 98% crystallinity was produced from the metakaolinization method within 8 h, while Na-X with 96% crystallinity was generated from the fused-metakaolinization (fusion) method within 48 h. In the fusion method, sodalite was formed at or beyond 48 h of hydrothermal reaction, while in the metakaolinite method, apart from a slight decrease in intensities of XRD peaks, no phase change was observed even after 168 h of hydrothermal reaction. Modification of the synthesis gel by increasing the Si/Al molar ratio via addition of fumed silica resulted in mixed zeolite products via the metakaolinite method, while Na-Y was the major product for the fusion method. Except for Na-A, all zeolite products had high surface area of up to 600 m^2/g and micropore volume of 0.18 cm^3/g. Our findings demonstrate the crucial role of the pre-treatment step in the synthesis of zeolites from clay minerals, and that a variety of high quality zeolites are achievable via choice of pre-treatment protocols.

Key words; Kaolinite, metakaolinite, fused-metakaolinite, Zeolite Na-A, Zeolite Na-X, Zeolite Na-Y, Fumed silica

1. Introduction

Zeolites are crystalline porous aluminosilicate materials built from tetrahedral network of silica $[SiO_4]^{-4}$ and alumina $[AlO_4]^{-5}$ ions linked to each other by the sharing of oxygen atoms [1]. Zeolites exist in natural as well as synthetic form, with the latter being more commonly used due to their purity and uniform particle size. The arrangement of silica and alumina tetrahedral leads to the creation of voids of varying dimensions that are usually occupied by charge balancing cations and water of hydration [2]. Zeolites, especially those of the faujasite (FAU) and Linde-type A (LTA) category, are useful in catalysis [3, 4], adsorption [5] and ion exchange [6] applications. The preparation of zeolites can be challenging, and current synthesis methods generally tend to use expensive sources of silica and alumina, which increases the cost of zeolites. Attempts have been made to synthesize zeolites from alternative cheaper sources of silica and alumina such as clay minerals [7, 8], fly ash [9], rice husks [10] as well as sewage sludge ash [11]. Kaolinite clays, in particular, are attractive as starting materials due to their purity and high silica and alumina content. Kaolinite has Si/Al molar ratio of 1, which is conducive for the synthesis of zeolite Na-A. Rios et al. [12, 13] and Kallie and Lipids [14, 15] prepared zeolites via reaction of raw kaolinite with NaOH. However, kaolinite did not fully dissolve in the alkaline solution resulting in incomplete conversion to zeolite and a mixed phase product consisting of a mixture of sodalite and cancranite products. The less reactive crystalline form of kaolinite may be converted to a more reactive amorphous phase via the metakaolinization process that involves calcination at temperatures above the dehydroxylation temperature of kaolinite. The challenge with this approach is that kaolinite clays exist in a variety of grades with varying content of impurities such as muscovite, mica and quartz. The quartz impurity is thermally stable and is, therefore, not easily broken down under metakaolinization conditions [16]. On the other hand, calcination of kaolinite at high temperature in alkaline media, via the so-called fusion process, completely destroys the kaolin structure [17] and also promotes the dry reactions of other mineral phases present (such as quartz) leading to high dissolution of aluminate and silicate products [18].

To date, the reported use of the fusion method prior to hydrothermal synthesis with kaolinite as starting material yielded products ranging from Na-A [13, 18], a mixture of zeolites [19] or Na-X when the starting material has high Si/Al ratio [8, 20, 21]. At the present time, despite the attraction of using kaolinite as starting material for zeolite synthesis, little is known as to why there is variation in the products obtained. In this work, we report the effect of metakaolinization and fused-metakaolinization on the synthesis of a variety of zeolites via hydrothermal crystallization using kaolinite clays with high quartz content. The synthesis conditions, i.e, calcination and fusion, gel composition and hydrothermal synthesis were similar for the two methods so as to specifically explore the influence of the chosen pre-treatment method, namely metakaolinization verses fused-metakaolinization. The effect of synthesis time and Si/Al ratio of the synthesis gel were also investigated. The raw kaolinite clay material, as well as the products were fully characterized by XRD, FTIR, BET, SEM and TGA analysis.

2. Materials and Methods

2.1. Materials

The clay used in this study was a white mineral powder supplied by the Department of Inorganic Chemistry, University of Yaoundé 1 - Cameroon. Chemical analysis of the clay showed that it was a kaolinite clay mineral with high quartz content (i.e., SiO_2, Al_2O_3, Fe_2O_3, TiO_2, CuO and K_2O of 53.51, 43.59, 2.37, 1.71, 0.84 and 0.36 wt % respectively). Sodium hydroxide (NaOH) pellets, 99%, sodium silicate pentahydrate ($Na_2SiO_3.5H_2O$), ≥ 97%, and fumed silica powder (SiO_2) of 0.2-0.3 μm particle size were obtained from Sigma Aldrich Chemicals. Deionized water was prepared using an Elga PURELAB Option 4463 water deionizer.

2.2. Zeolite Synthesis

Two synthesis routes, i.e. metakaolinization (MK) or fused-matakaolinization (F-MK), based on modifications of previous reports [7, 13] were used. Initially, synthesis gel containing Na_2O:SiO_2:Al_2O_3:H_2O at molar ratio of 3.5:2.1:1:143.2 was used for both the MK and F-MK methods. For the MK route, kaolinite clay was calcined by heating at 10 °C/ min to 750 °C and then holding at this temperature for 8 h. The required amount of calcined MK clay was then mixed with 43 ml of 2.7 M NaOH solution in a 50 ml polytetrafluoroethylene (PTFE) bottle. In the F-MK route, dry kaolinite clay was mixed with NaOH pellets (to meet the above synthesis ratio) by grinding in an agate motor before heating the resulting mixture as described above (i.e., at 750 ^{o}C for 8 h). The resulting F-MK product was weighed and mixed with deionized water in a 50 ml PTFE bottle. Both synthesis batches were then stirred at 25 °C for 4 h at 600 rpm to give a homogeneous gel before allowing the gel to age under static conditions for 24 h at 25 °C. After seeding, the gels were placed in a box furnace to crystallize at 100 °C under static conditions for different periods of time from 8 h to 240 h.

The effect of Si/Al was investigated by modifying the Na_2O:SiO_2:Al_2O_3:H_2O molar ratio of the gel to 10:1:7.98:120 by addition of fumed silica. Specifically, 5.0 g of MK, 32.16 g sodium metasilicate pentahydrate and 28.0 ml H_2O, or 5 g of MK, 7.69 g NaOH, 10.17 g fumed silica and 44.5 ml H_2O were used. The effect of crystallization time, in the range of 8 h to 240 h, was also studied for both routes.

2.3. Characterization

Powder XRD patterns were obtained in continuous mode with 2θ scan step size of 0.026° using a PANalytical X-Pert Pro X-ray powder diffractometer (Almelo, Netherlands) employing Cu-Kα radiation. Zeolite phases in the reaction products were identified by comparison with commercially available zeolites and the zeolite database from the International Zeolite Association [22]. The percentage crystallinity was estimated by comparing the peak areas of ten selected peaks (at 2θ of 6.15°, 10.06°, 15.51°, 20.11°, 23.34°, 26.67°, 30.35°, 30.98°, 32.06° and 33.61° for Na-X, and at 7.27°, 10.24°, 16.17°, 21.71°, 24.05°, 27.17°, 30.88°, 32.59°, 33.43° and

34.21° for Na-A), with those of commercially available zeolite 13X and zeolite 4A, respectively. Infra-red spectroscopy was performed to monitor the presence of functional groups using a Bruker Alpha Attenuated Total Reflectance - Fourier Transform Infrared (ATR-FTIR) spectrometer. Thermogravimetric analysis (TGA) was performed using a TA Instruments SDT Q600 thermal analyzer by heating samples at 10 °C/min under flowing air (100 mL/min) up to 1000 °C. The morphology of the samples was explored via scanning electron microscopy (SEM) using a FEI Quanta 200 3D Dual Beam FIB microscope. Elemental composition was obtained using an energy dispersive spectrometer (EDS) during SEM analysis. The textural properties of the produced zeolites were analyzed using a Micromeritics 3FLEX sorptometer employing N_2 gas as a sorbate at liquid nitrogen temperature. The samples were outgassed prior to analysis under vacuum at 230 °C for 16 h. The surface area was calculated using the Brunauer-Emmett-Teller (BET) method. The total pore volume was calculated from the nitrogen uptake at close to saturation pressure while micropore surface area and micropore volume were determined from t-plot analysis.

3. Results and Discussion

3.1. Analysis of clay minerals used as starting materials

Figure 1a shows the XRD pattern of the raw clay mineral. The peaks at 2θ of 12.44° and 24.86° are characteristic of the kaolinite phase while those at 2θ of 20.87°, 26.67°, 36.60°, 39.49°, 42.49° and 45.82° correspond to quartz phases. The expected broad hump at 2θ of 13° - 30° for MK, corresponding to newly formed amorphous aluminosilicates, was masked by the intense quartz peaks. The FT-IR spectra in Figure 1b reveals four bands, at 3620 cm^{-1} due to stretching vibrations of inner –OH groups (Al-OH), and others (at 3654, 3667 and 3687 cm^{-1}) due to stretching vibrations of surface –OH groups, which are characteristic of the triclinic layer structure of kaolinite clays [23]. Other IR bands at 1025 cm^{-1} (Si-O stretching), 525 (Si-O-Si bending) as well as doublet bands at 789 and 751 cm^{-1} (due to Si-O from quartz) have also been previously observed [24]. The Si-O bands shifted to higher wavenumbers following metakaolinization with the broad band centered at 1049 cm^{-1} representing amorphous aluminosilicate stretching vibrations, and a peak at 451 cm^{-1} due to aluminosilicate bending vibrations. All other bands in the raw kaolinite mineral were not observed after metakaolinization except those of quartz, which were still visible within the broad band at 780 cm^{-1}. The peaks and bands for the quartz and amorphous aluminosilicate phases were not observed in the XRD pattern and the FTIR spectrum respectively of F-MK. Instead, both XRD and FTIR showed emergence of new crystalline phases. The SEM image in Figure 1c for the raw clay mineral depicts a pseudohexagonal platy morphology typical of kaolinites [25] while that in Figure 1d correspond to the amorphous MK. Elemental analysis indicated that SiO_2 (53.5 wt%) and Al_2O_3 (43.6 wt%) were the main oxides in the kaolinite clay mineral. Trace amounts of other oxides of titanium, iron, potassium and calcium were also detected.

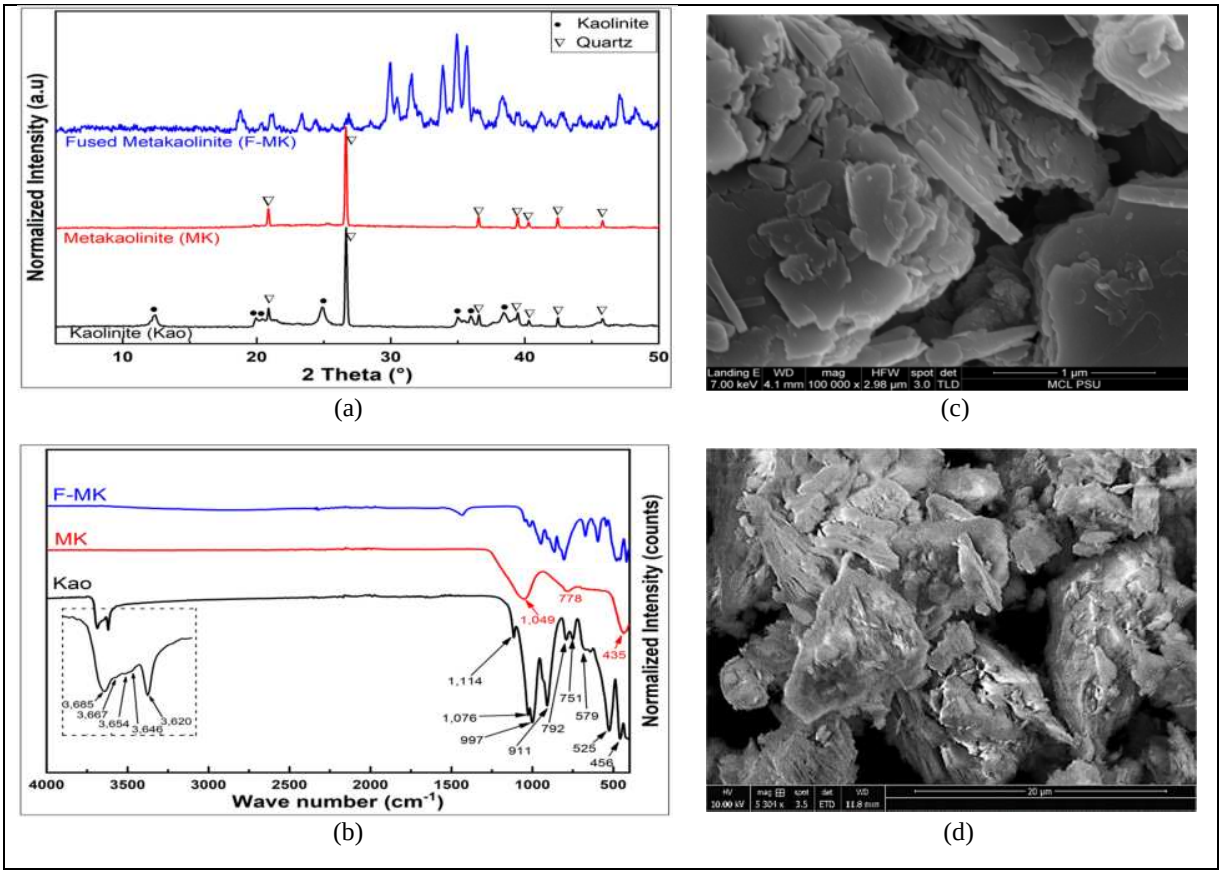

Figure 1; Characterization of kaolinite (Kao), metakaolinite (MK) and fused-metakaolinite (F-MK); (a). XRD patterns of Kao, MK and F-MK, (b). FTIR spectra of Kao, MK and F-MK, (c). SEM image of Kao, (d). SEM image of MK.

3.2. Hydrothermal Crystallization Products

For the metakaolinite-derived product, apart from the quartz peaks in the XRD pattern originating from the parent kaolinite, other peaks appeared at 2θ of ca. 7.27°, 10.24°, 16.17°, 21.71°, 24.05°, 27.17°, 30.88°, 32.59°, 33.43° and 34.21° (Figure 2a) that are characteristic of Na-A zeolite [22]. The percentage crystallinity of the synthesized Na-A was 88.1%. SEM images revealed cubic particles as large as 3.5 µm with truncated edges, and some inter-growth (Figure 2b), which further confirms the presence of zeolite Na-A products. Figure 2d shows the XRD pattern of products from the fused-metakaolinite F-MK) method. Zeolite Na-X with 95.9% crystallinity, characterized by the presence of the 2θ peaks at 6.15°, 10.06°, 15.51°, 20.11°, 23.34°, 26.67°, 30.35°, 30.98°, 32.06° and 33.61° [22], was the main product. It is noteworthy that the quartz peaks were not observed for the product of the F-MK route. From the elemental analysis data, shown in Table 1, the chemical formula of the synthesized Na-X was calculated to be; $Fe_{0.74}Ti_{1.80}K_{0.42}$ $Na_{75.06}Al_{85.79}Si_{98.14}O_{367.89}$, which is consistent with other reports [26, 27]. The SEM images of Na-X in Figure 2d reveal octahedral-like crystals, which are characteristic of zeolite X, with smaller crystal size compared to those of synthesized Na-A (Figure 2c). Figures 2b and 2e show the FTIR spectra of the synthesized Na-A and Na-X, respectively. The bands at ca. 3360 and 1641 cm^{-1} are due to hydroxyl stretching and bending vibrations respectively, associated with water of hydration [28]. For Na-A, the broad band at 1200-900 cm^{-1} due to

amorphous aluminosilicates shifts to lower wave numbers as crystalline Si-O-Si, Si-O-Al and Al-O-Al bonds are formed. For Na-X (Figure 2f), there is s general shift of the bands of fused kaolinite to high wave numbers. The peaks at 1000 cm^{-1}, 667 cm^{-1} and 450 cm^{-1} arise from the asymmetric stretching, symmetric stretching and bending vibration, respectively, of T–O bonds in TO_4 tetrahedral [29]. The band at ca. 550 cm^{-1} corresponds to the double membered rings, D4R and D6R, for zeolites A and X, respectively [30].

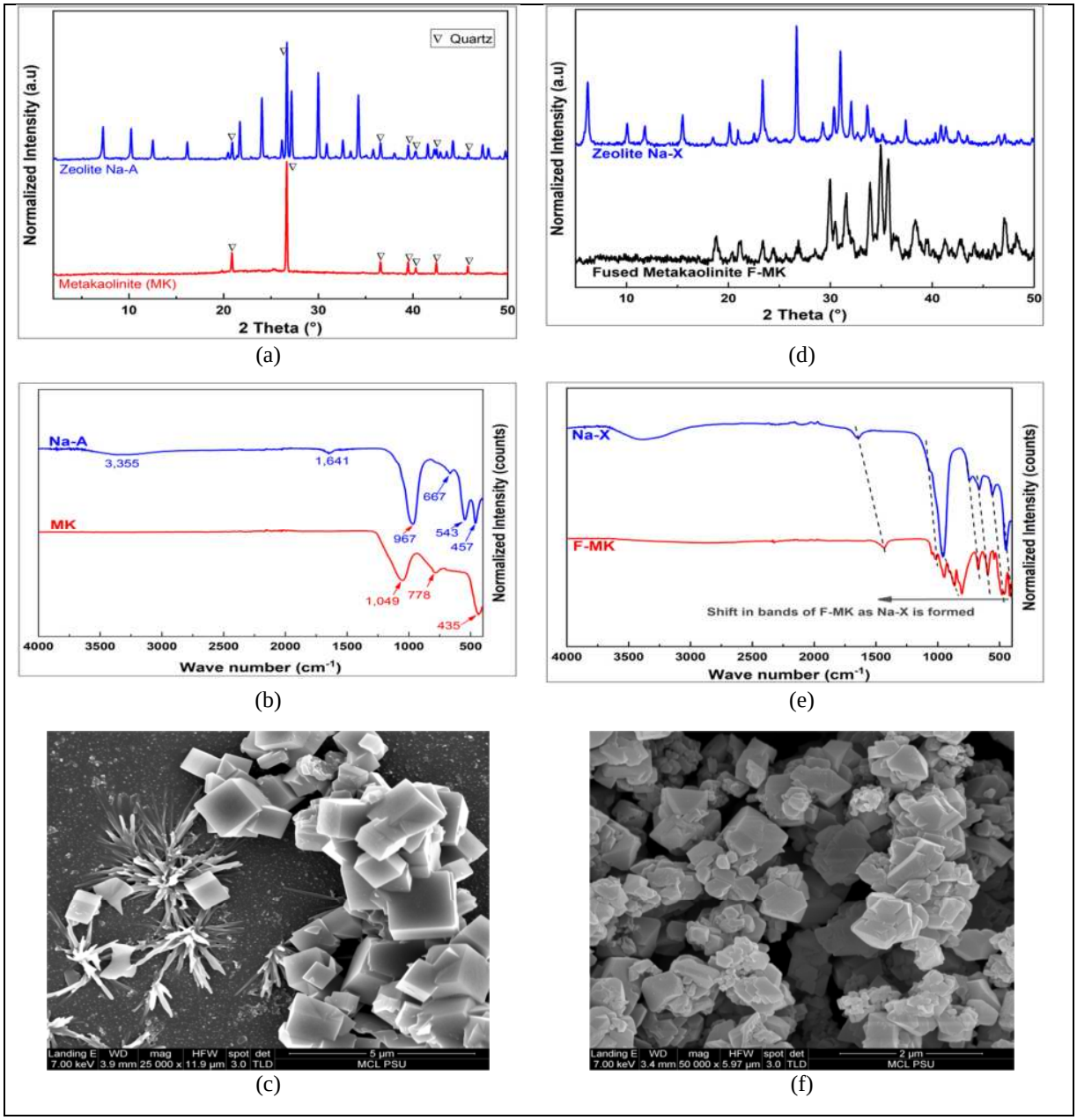

Figure 2; XRD patterns, FTIR spectra and SEM images; (a). XRD pattern of transformation of MK product, (b). FTIR spectra of transformation of MK product, (c). SEM image of MK product, (d). XRD pattern of transformation of F-MK product, (e). FTIR spectra of transformation of F-MK product, (f). SEM image of F-MK product.

Table 1: Chemical composition of kaolinite clay used as starting material and synthesized zeolites.

	Percent oxide (wt% MO_x)							
	Na_2O	Al_2O_3	SiO_2	K_2O	TiO_2	Fe_2O_3	CuO	Si/Al
Kaolinite Clay	0	43.59	53.51	0.36	1.71	2.37	0.84	1.04
Na-X	18.08	33.99	45.82	0.16	1.12	1.83	0.81	1.14
Na-A	19.60	33.63	44.36	0.28	1.49	1.87	0.79	1.12

The synthesized zeolites were found to be stable up to 800 °C as shown by the TGA curves in Figure 3. Up to 17% weight loss was observed and is attributable to absorbed water within the framework. As revealed by the derivative of the heat flow curve, the water loss occurred in two exothermic steps, the first at 60-180 °C is due to water of hydration and water within the crystal lattice. This is followed by a slower second step that commences at ca. 200 ^{o}C and is complete at 400 °C, which is attributed to loss of adsorbed water from within the zeolite micropores [31]. The second step was slower for Na-A zeolites due to there being a greater diffusion barrier during desorption of water through the narrower channels of this small pore zeolite.

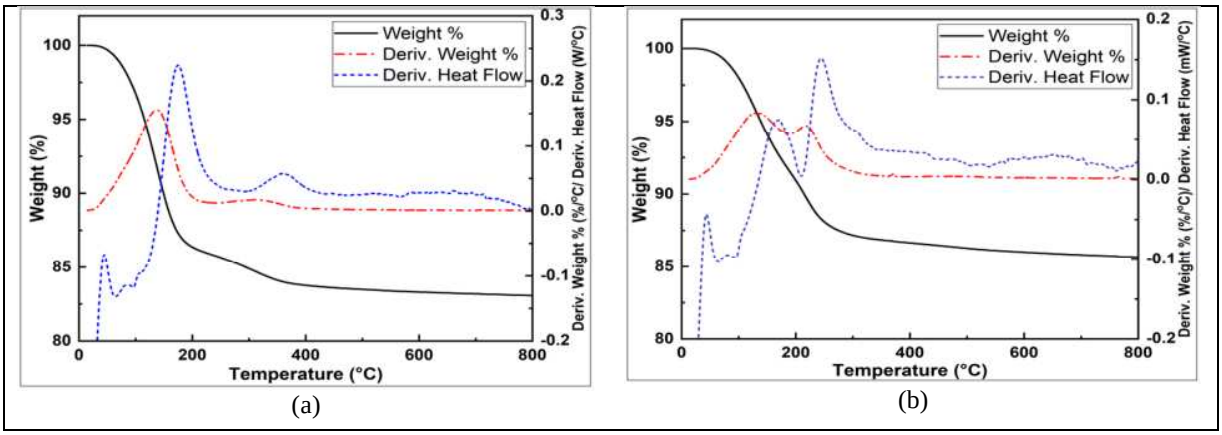

Figure 3; TGA curves of hydrothermal crystallization products prepared via the; (a) metakaolinization and (b) fused-metakaolinization routes.

Porosity analysis results are given in Figure 4 and Table 2. Reversible Type I adsorption isotherms were obtained for the products of F-MK method. This is an indication that the products are microporous with narrow micropores [32], according to the steep slope of the isotherm at very low relative pressure (P/P_0), which is characteristic of zeolite-adsorbate interactions in narrow micropores resulting in filling of micropores at such low relative pressure. The zeolites synthesized via the fusion route have high surface area of 473 to 579 m^2/g. They also had two size range micropores; the inner pores of sodalite cage openings of size 0.59 nm and the outer pores of size 0.71 nm or 0.73 nm, along with an associated high micropore volume of 0.15 to

0.18 cm^3/g. On the other hand, we observed low adsorption for Na-A due to its small pores of size 0.42 nm [33], which hinder the sorption of N_2 molecules. We note that due to the very low porosity detected for Na-A (as a result of the N_2 molecule being too large to enter the Na-A pores), the intensity of the pore size distribution plot (Figure 4b) is so low that it is barely above the baseline. Furthermore we also note that the fact that the N_2 molecules cannot readily enter the Na-A pores means that the small pore channels should not be detectable, which is consistent with the very low intensity of the pore size distribution plot.

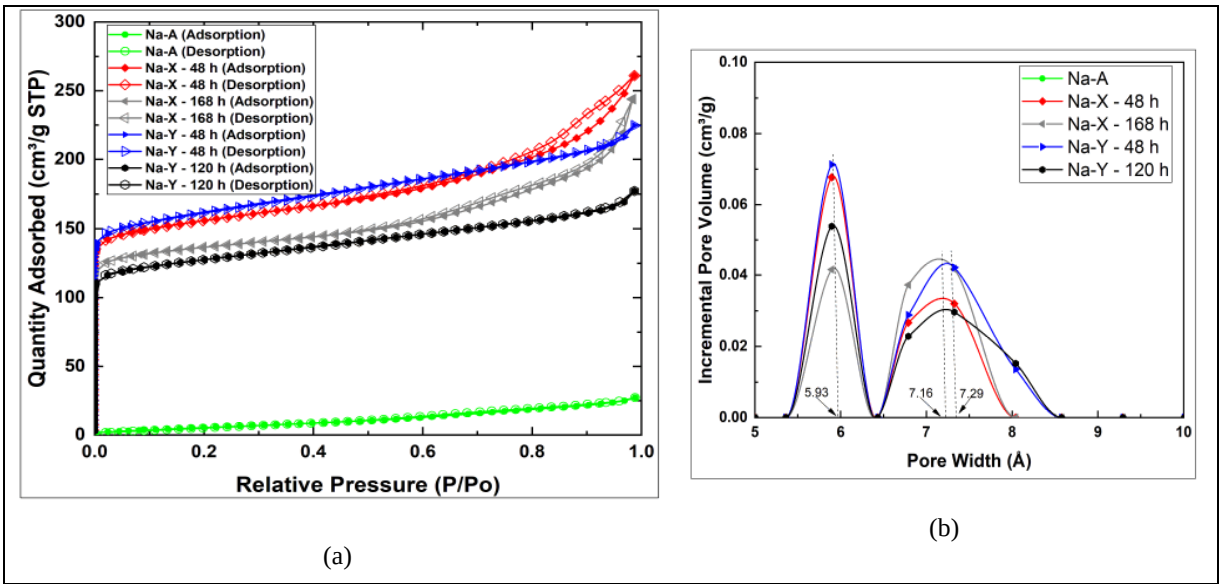

(a) (b)

Figure 4; BET analysis of synthesized zeolites; (a). Nitrogen sorption isotherms and (b). Pore size distribution curves.

Table 2: Textural properties of kaolinite clay and synthesized zeolites

	Surface area (m^2/g)	M_{icro} (m^2/g)	S_{Ext} (m^2/g)	V_{Micro} (cm^3/g)
Kaolinite Clay	12		12	
Na-A	18		38	
Na-X 48 h	579	445	134	0.18
Na-X 168 h	510	413	98	0.17
Na-Y 48 h	600	445	154	0.18
Na-Y 120 h	473	355	118	0.15

Key: S_{Micro} - micropore surface area, S_{Ext} - external surface area while V_{Micro} - micropore volume.

3.3. Formation of LTA versus FAU zeolite

The surface morphology for metakaolinite under SEM, Figure 1d, reveals the presence of pseudohexagonal flakes even after high thermal treatment of kaolinite clay from which it is derived. For the hydrothermal synthesis route using metakaolinite, although the nominal Si/Al

molar ratio in the synthesis gel is more than 1, most of the silica might be present in the form of quartz (Figure 1a) meaning that the actual amount of silica available as primary building units in the sodium aluminosilicate gel is lower than the calculated nominal concentration. Such a low concentration of silica would be conducive for the transformation of the aluminosilicate gel to zeolite Na-A. On the other hand, for the fused-metakaolinite route, in addition to the complete dissolution of kaolinite clay [17], the high alkaline conditions of the fusion method that utilizes NaOH at high temperatures, increases the concentration of silica ions by breaking down crystalline quartz. The synthesis mixture in the fusion method is thus richer in silicate ions, which is conducive for the transformation of the aluminosilicate gel to zeolite Na-X products.

Alternatively, it is possible that the formation of Na-X seeds occurs early during the fusion method, which encourages the formation of zeolite Na-X. Unlike the amorphous phase of the MK route, the presence of new peaks in the XRD pattern of F-MK products, (Figure 2d), is an indication of the crystals formed during the fusion step. The peaks at 2θ between 23° and 32° for F-MK also tend to shift to higher 2θ values as products are formed during the hydrothermal crystallization step. In addition, the FTIR spectra of the fusion product and its F-MK precursor (Figure 2e) are comparatively identical with the spectral bands of the later shifting to higher wave numbers as the zeolite products are formed. Therefore, the higher temperature dry reaction between kaolinite-derived aluminosilicates with NaOH may result in the formation of secondary and/or tertiary building units with D6R structure that can act as seeds leading to the synthesis of faujasites under conditions that are similar to those that lead to LTA zeolites via the MK route.

3.4. Effect of crystallization time

The hydrothermal synthesis (crystallization) time was varied between 8 and 168 h for zeolite Na-A, and between 8 and 240 h for Na-X. Figure 5 shows the XRD patterns of the resulting products prepared at varying hydrothermal crystallization periods. In the MK method (Figure 5a), apart from quartz, zeolite Na-A of more than 90% crystallinity was generated within 8 h of hydrothermal crystallization. It is noteworthy that no phase transition was observed up to 168 h. The only change observed was on the drop in crystallinity to less than 70% after 120 h which is also reflected by the slight reduction of XRD peak intensities with time (Figure 5a). This is in contrast to other reports where a more stable hydroxysodalite phase was formed just after 48 h [28]. On the other hand, for the F-MK method, zeolite Na-A was formed alongside Na-X at lower crystallization times. As crystallization time increased, Na-A was transformed via dissolution to form greater amounts of Na-X [12], with Na-X being the abundant phase after 48 h via the process of Ostwald's ripening [34]. Further increase in crystallization time resulted in formation of a hydroxysodalite zeolite phase. The appearance of Na-X at low reaction times at the low gel Si/Al ratio of 1 is further proof of the formation of Na-X seeds during the fusion step. The presence of a stable phase of Na-X in the hydrothermal synthesis gel makes it easier for the Na-A phase to dissolve into solution resulting in formation of more Na-X via Ostwald's ripening. In addition, unlike in the MK route, the high Si/Al ratio in the synthesis gel for the F-MK route made the transformation to sodalite possible at longer hydrothermal crystallization periods.

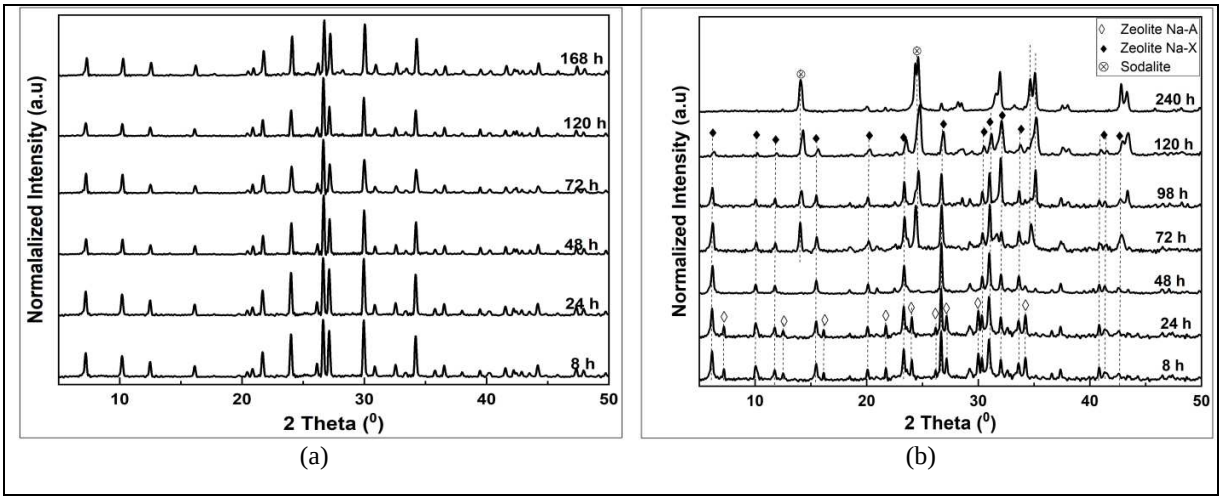

Figure 5; Effects of crystallization time on zeolite synthesis via; (a). MK route (Na-A zeolite) and (b). F-MK route (Na-X zeolite).

3.5. The effect of Si/Al ratio

The silica to alumina ratio of the synthesis gels was increased in an attempt to synthesize high silica zeolites. Figure 6 shows the XRD patterns of the products obtained at varying Si/Al molar ratio for the MK and F-MK methods. In the MK method, a mixture of zeolites was obtained, while zeolite Na-Y was the major product for the F-MK route. The peaks at 2θ of 6.38°, 10.21°, 12.10°, 15.86°, 20. 53°, 27.48°, 31.30° and 34.66° are characteristic of zeolite Na-Y [22]. Other peaks that can be ascribed to Na-X (at 18.64°, 23.61° and 26.78°), Na-P (at 12.47°, 17.75°, 28.15°and 40.23°) and analcime (at 24.28°, 25.97°, 36.89° and 42.59°) are also observed. The large hump at 2θ of 18 - 45° in Figure 6a can be attributed to unreacted amorphous phase in the starting MK precursor, which suggests that more time is necessary for the complete reaction (transformation) of the sodium aluminosilicate gel to occur in the MK route. This hump was not observed in the XRD patterns of F-MK products. It is likely that faujasite seeds that formed during the fusion step (for the F-MK route) accelerated the reaction rate so as to result in a relatively pure Na-Y phase. Increasing the Si/Al ratio also leads to an increase in pore opening of zeolite crystals from 0.71 nm to 0.73 nm (Figure 4b).

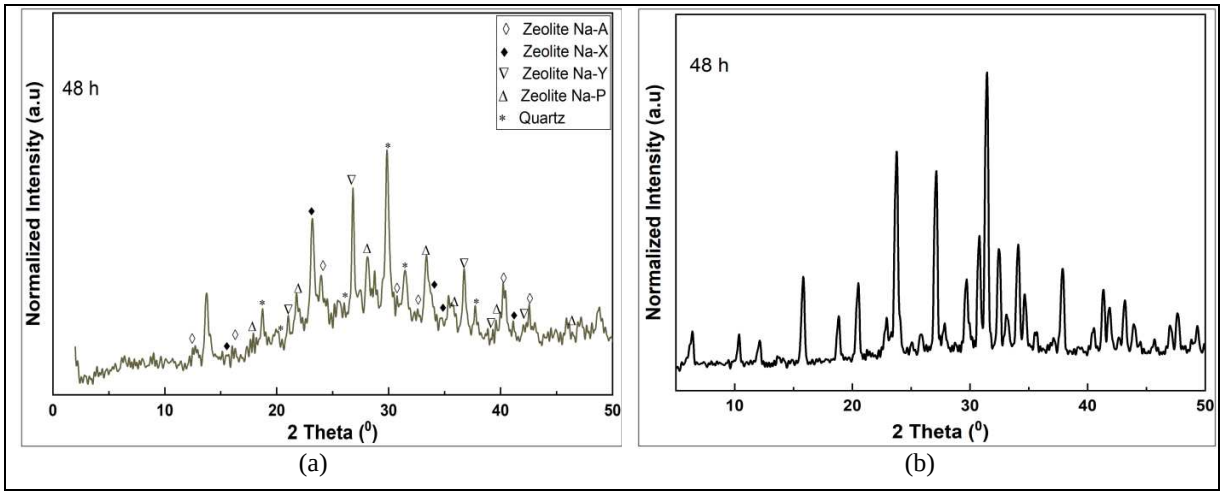

(a) (b)

Figure 6; Effects of synthesis gel Si/Al molar ratio on zeolite synthesis process (via addition of fumes silica) for; (a). MK route products and (b). F-MK route products.

4. Conclusion

In this work, FAU and LTA zeolites of high crystallinity were successfully synthesized from kaolinite clay minerals with high quartz content. For gels of similar composition and under identical synthesis conditions, the resulting zeolite type depended on which pre-treatment method, namely MK (metakaolinization) or F-MK (fused-metakaolinization) was applied to the natural clay prior to the hydrothermal crystallization step. At lower Si/Al ratio, the synthesized zeolite was stable and independent of crystallization time for the MK route, while the zeolite generated from the F-MK route depended on crystallization time. A mixture of zeolites (Na-X, Na-P, analcime) were obtained in the MK route when the Si/Al ratio of the synthesis gel was greater than 1. In contrast, for the F-MK route, Na-Y was the dominant phase at high gel Si/Al ratio. The hydrothermal crystallization time required for the preparation of faujasite zeolites from kaolinite clays was significantly reduced if the fusion (i.e. fused-metakaolinization) route is followed. The fusion step generates zeolite seed crystals with faujasite structures during the dry reaction between kaolinite-derived aluminosilicates and NaOH. These seeds are utilized as building blocks for further zeolite formation during hydrothermal crystallization, and act to favour the formation of high purity and crystallinity Na-X and, at high silicate ion concentration (Si/Al > 1), zeolite Na-Y is generated. This work shows that high quality FAU or LTA zeolites can be obtained from the abundant and inexpensive natural aluminosilicate resources and wastes by choice of either the fusion or metakaolinization routes with no change in hydrothermal synthesis conditions.

Acknowledgement

We thank the Royal Society (ACBI programme grant number AQ150029) for funding this work. We also thank all the Materials Chemistry research group members at School of Chemistry, University of Nottingham for assistance with various aspects of this work.

References

[1] L.B. McCusker, C. Baerlocher, Zeolite Structures, in: J. Čejka, H. van Bekkum, A. Corma, F. Schüth (Eds.) Studies in Surface Science and Catalysis, Elsevier 2007, pp. 13-37.
[2] E.B.G. Johnson, S.E. Arshad, Appl. Clay Sci. 97-98 (2014) 215-221.
[3] A.J. O'Malley, C.R.A. Catlow, Sorbate Dynamics in Zeolite Catalysts, in: F. Fernandez-Alonso, D.L. Price (Eds.) Experimental Methods in the Physical Sciences, Academic Press 2017, pp. 349-401.
[4] E.F. Sousa-Aguiar, Chapter 6 - Y Zeolites as a Major Component of FCC Catalysts: Main Challenges in the Modification Thereof, in: B.F. Sels, L.M. Kustov (Eds.) Zeolites and Zeolite-Like Materials, Elsevier, Amsterdam, 2016, pp. 265-282.
[5] R. Dehghan, M. Anbia, Fuel Process. Technol. 167 (2017) 99-116.
[6] H. Figueiredo, C. Quintelas, J. Hazard. Mater. 274 (2014) 287-299.
[7] C.A. Ríos, C.D. Williams, O.M. Castellanos, Ing. y competitividad, 14 (2012) 125-137.
[8] N.M. Musyoka, R. Missengue, M. Kusisakana, L.F. Petrik, Appl. Clay Sci. 97-98 (2014) 182-186.
[9] V. Volli, M.K. Purkait, J. Hazard. Mater., 297 (2015) 101-111.
[10] Y. Cheng, M. Lu, J. Li, X. Su, S. Pan, C. Jiao, M. Feng, J. Colloid Interface Sci. 369 (2012) 388-394.
[11] Y. Zhang, Z. Leng, F. Zou, L. Wang, S.S. Chen, D.C.W. Tsang, J. Clean Prod. 172 (2018) 686-695.
[12] C.A. Rios, C.D. Williams, M.J. Maple, BISTUA, 5 (2007) 15-26.
[13] C.A. Ríos, C.D. Williams, M.A. Fullen, Appl. Clay Sci. 42 (2009) 446-454.
[14] L. Heller-Kallai, I. Lapides, Appl. Clay Sci. 35 (2007) 99-107.
[15] I. Lapides, L. Heller-Kallai, Appl. Clay Sci. 35 (2007) 94-98.
[16] H.M. Zhou, X.C. Qiao, J.G. Yu, Appl. Clay Sci. 80-81 (2013) 176-181.
[17] N. Li, T. Li, H. Liu, Y. Yue, X. Bao, Appl. Clay Sci. 144 (2017) 150-156.
[18] L. Ayele, J. Pérez-Pariente, Y. Chebude, I. Díaz, Appl. Clay Sci. 132-133 (2016) 485-490.
[19] C. Belviso, F. Cavalcante, A. Lettino, S. Fiore, Appl. Clay Sci. 80-81 (2013) 162-168.
[20] M. Mezni, A. Hamzaoui, N. Hamdi, E. Srasra, Appl. Clay Sci. 52 (2011) 209-218.
[21] Y. Ma, C. Yan, A. Alshameri, X. Qiu, C. Zhou, D. li, Adv. Powder Technol., 25 (2014) 495-499.
[22] Ch. Baerlocher, L.B. McCusker, Database of Zeolite Structures. http://www.iza-structure.org/databases/ (accessed June 8, 2018)
[23] P. Djomgoue, D. Njopwouo, J. Surf. Eng. Mater. Adv. Technol. 3 (2013) 275-282.
[24] B.J. Saikia, G. Parthasarathy, J. Mod. Phys. 1 (2010) 206-210.
[25] H. Hanlie, C. Wang, K. Zeng, K. Zhang, K. Yin, Z. Li, Clays Clay Miner. 60 (2012) 240-253.
[26] D.H. Olson, Zeolites, 15 (1995) 439-443.
[27] H. Guesmi, P. Massiani, Catal. Today, 177 (2011) 25-30.

[28] H. Tounsi, S. Mseddi, S. Djemel, Phys. Procedia, 2 (2009) 1065-1074.
[29] R. Belaabed, S. Elabed, A. Addaou, A. Laajab, M.A. Rodríguez, A. Lahsini, Bol. Soc. Esp. Ceram. Vidr. 55 (2016) 152-158.
[30] W. Mozgawa, W. Jastrzębski, M. Handke, J. Mol. Struct., 744-747 (2005) 663-670.
[31] Ö.Ç. Duvarcı, Y. Akdeniz, F. Özmıhçı, S. Ülkü, D. Balköse, M. Çiftçioğlu, Ceram. Int., 33 (2007) 795-801.
[32] M. Thommes, K. Kaneko, A. V. Neimark, J. Olivier, F. Rodriguez-Reinoso, J. Rouquerol, K. Sing, Pure and Appl. Chem. 87 (2015) 1051-1069.
[33] J. Bronić, A. Palčić, B. Subotić, L. Itani, V. Valtchev, Mater. Chem. Phys., 132 (2012) 973-976.
[34] H. Greer, P.S. Wheatley, S.E. Ashbrook, R.E. Morris, W. Zhou, J. Am. Chem. Soc., 131 (2009) 17986-17992.